FLUORESCENCE TEMPERATURE MEASUREMENT OF OPTICAL THERMOCAVITATION

Banks, D.[1], Zhang, B. [1 2], Akbarimoosavi, S. M. [1], Devia-Cruz, L. [1], and Aguilar, G. [1] *
*Author for correspondence
[1] Department of Mechanical Engineering,
University of California, Riverside,
Riverside, 92521,
California, USA,
E-mail: gaguilar@engr.ucr.edu

[2] School of Energy and Power Engineering,
Xi'an Jiaotong University,
Xi'an, 710049,
P. R. China

ABSTRACT

While optical cavitation creates and directs potent localized flows non-intrusively, the resulting thermal dynamics are uniquely difficult to characterize. The acoustic shockwaves produced by cavitation damage submersed sensors near enough to effectively measure cavitation dynamics. The bubble lifetime is on the order of tens of microseconds, demanding a high sampling rate which is difficult and costly to achieve via infrared imaging, and requires fragile micro-scale temperature sensors. Planar laser-induced fluorescence provides an alternative technique to explore the thermal effects of optical cavitation. The temperature field around the cavitation bubble can be measured non-intrusively with this method using a high speed video camera.

A 440 nm continuous laser sheet excites rhodamine B dye to fluoresce. The intensity of the fluorescence is correlated to the liquid temperature. A Miro 310 camera is used to record the fluorescent intensity while cavitation is induced by a focused continuous wave 810 nm laser – a wavelength that does not produce fluorescence in rhodamine. The temperature field is characterized qualitatively at very high frame rates using a shadowgraph method, and quantified by measuring the fluorescent intensity during cavitation.

INTRODUCTION

Cavitation induced by continuous wave (CW) lasers is a novel method to produce and influence liquid flow non-intrusively at targeted locations. The rapid growth and collapse of the bubble strongly agitates the surrounding liquid. Particularly in microfluidic devices, turbulent mixing is challenging to create, but would be invaluable for micro-analysis and lab-on-a-chip systems [1]. Further, thermocavitation bubbles formed near a solid boundary can enhance convective heat transfer. Unique dynamics in the bubble collapse – particularly an asymmetry where a jet pulls the bubble pole towards the nearest solid surface – draw liquid toward the surface. Known as microstreaming, this dynamic has been exploited using acoustically vibrated bubbles in micro-scale mixing applications, facilitating fast homogeneous mixing in otherwise unmixed reservoirs [2]. Based on these principles, optical cavitation should be able to enhance convective cooling by pulling cold liquid from an unheated bulk fluid towards a hot boundary.

To evaluate the effectiveness of optical cavitation in this application, the temperature field surrounding the bubble must be measured. Direct temperature measurement is prohibited by the acoustic shockwaves typically produced upon bubble formation and collapse. Any sensor fast enough to characterize cavitation dynamics is by necessity small and exposed, making it susceptible to such damage.

Further, characterizing a temperature field using point-response sensors is difficult and intrusive. Infrared cameras avoid the hazards associated with cavitation, but lack the time resolution to observe the microsecond timescales of cavitation bubble dynamics.

Laser-induced fluorescence temperature measurement offers a novel option to overcome the challenges of characterizing the cavitation temperature field. This study explores that capability using the temperature-sensitive fluorescing rhodamine B dye and a high speed digital video camera. Using a light sheet as the excitation source, planar laser induced fluorescence (PLIF) allows simultaneous observation of the cavitation bubble and the temperature surrounding it. PLIF is implemented in an existing optical setup used to produce and characterize cavitation bubbles. PLIF is relatively inexpensive, and using high speed video, it can achieve the necessary temporal resolution.

Optical cavitation was first observed when a ruby pulsed laser was focused into water by Carome, et al [3]. Since then, cavitation has been induced by pulsed and continuous wave lasers [4, 5] and has seen applications in biomedicine [6], microfluidics [7], fluid composition studies [8], nanoscale engineering [9], and many others. Pulsed laser cavitation tends to be more commonly reported; the energy density of short-duration laser pulses often exceeds that of continuous lasers and can ionize the target liquid, readily nucleating a bubble [10]. CW laser cavitation, typically with a lower energy density, has not been seen to ionize the liquid and instead, in a relatively much slower process, superheats the irradiated volume to vaporization [11]. CW-induced cavitation can therefore be referred to as 'thermocavitation'.

In the context of thermocavitation, the heating process is extended and expanded significantly over the near-instantaneous dynamics of pulsed laser-induced cavitation. The optical energy absorbed by the liquid becomes sensible to heat

prior to cavitation. During this process, the refractive index of the working liquid is changed within the heated volume. In comparison, pulsed lasers induce phase change on the leading edge of the pulse, avoiding the comparatively slow heating around the laser focal volume in CW cavitation.

At first glance, thermocavitation as a cooling aid seems odd. Thermocavitation is a heating process - the focal volume is heated to near its spinodal limit [5]. Without somehow dispersing the added heat, any additional convective cooling will be negated. The fate of the energy used to produce cavitation determines cavitation's effectiveness as a cooling mechanism. Two approaches may reduce the heat involved in cavitation. First, to facilitate cavitation so it occurs after absorbing less energy. This can be accomplished using liquids that nucleate more easily by having a lower boiling point and/or latent heat. One example of this approach is the work of Rastopov and Sukhodolsky, who found that the optical energy required for cavitation in water-ethanol solutions decreased as the proportion of ethanol increased [12]. Increasing the concentration of ethanol in water lowers the boiling point and latent heat significantly.

The second approach is to ensure that the needed energy is converted to non-thermal forms after the bubble occurs. The cavitation process itself facilitates this dispersion. The majority of the energy driving cavitation is converted to acoustic energy. The shockwaves marking the formation and collapse of the bubble scatter nearly 75% of the absorbed laser energy [13]. This enables cavitation to work as a surface cooling mechanism.

CW thermocavitation has been observed to produce bubbles that collapse in a toroidal shape [14]. When a bubble forms near a heated solid boundary, the polar collapse jet will be comprised of colder liquid from outside the heated layer near the boundary. Following the collapse, some of the hot liquid at the boundary will be ejected from the nucleation site outward.

EXPERIMENTAL SETUP

Shadowgraph Imaging

Prior to quantitative temperature measurement using fluorescence, a form of shadowgraph imaging was used to qualitatively observe the temperature field during the cavitation process. Using a laser as illumination, the high speed video camera records a video of the cavitation process (Fig. 1). Since heated liquid has an altered refractive index over unheated liquid, and given the collimated nature of the laser light, heated regions within the cuvette appear as shadows and contours on video, as seen in Figure 2. For purposes of shadowgraph imaging, no rhodamine B was added to the solution – the absorption of rhodamine would have prevented laser light from reaching the camera.

Shadowgraph imaging was included in this study for two reasons. First, it provides a form of qualitative validation of the PLIF temperature field measurements. Although it does not confirm the measurement of the temperature itself, the distribution of heated liquid observed using both PLIF and shadowgraphy are similar. Second, because shadowgraph imaging uses direct illumination, video needs less exposure time and thus can be recorded at significantly higher framerates than the much less intense illumination provided by rhodamine B fluorescence. Shadowgraphy images are recorded at 10000 fps, whereas PLIF videos are an order of magnitude slower at 1000 fps. Shadowgraph videos can help fill in the gaps, so to speak, where PLIF may miss some of the short-duration dynamics of cavitation.

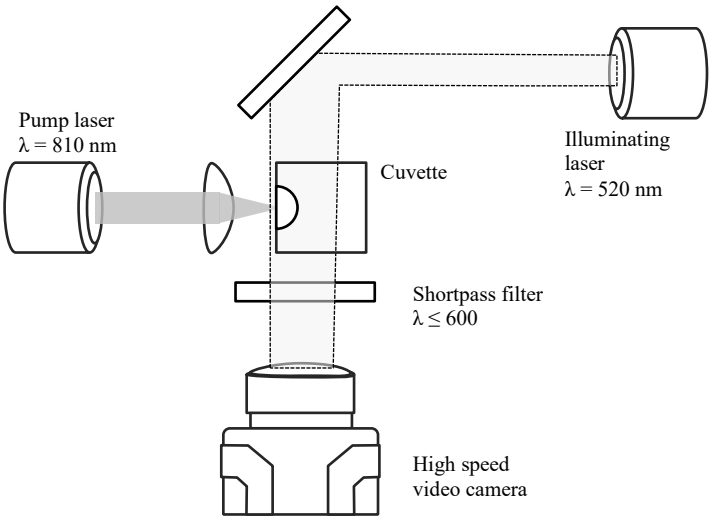

Figure 1 Shadowgraphy imaging experimental setup.

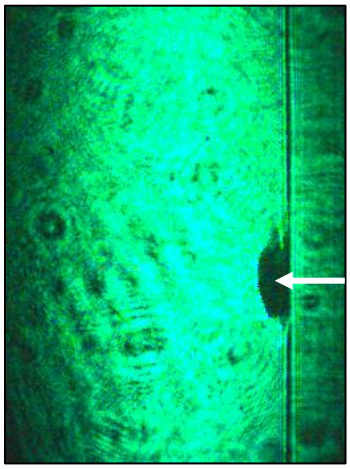

Figure 2 Shadowgraph image of thermal boundary layer on the cuvette wall due to spot heating. The vertical line on the right side is the wall, and the laser axis is centered on the arrow.

PLIF Apparatus

PLIF is reasonably simple in principle. Dye is irradiated by a certain wavelength of light, from a laser beam shaped into a sheet. Under this excitation, dye fluoresces at a different wavelength. Using a video camera and image analysis software, the intensity of fluorescence can be measured. This fluorescence can be correlated with the conditions of the dye: pressure, concentration, or shear. Certain dyes fluoresce with different intensity at different temperatures. Holding everything else approximately constant, then, the fluorescence can be used to measure the local temperature [15].

A solution of rhodamine B (R-B) dye in aqueous copper nitrate (CN) is the working liquid for this study, contained in a 1 cm by 1 cm by 4 cm glass cuvette. The cuvette is transparent on all sides in the visible and near-IR spectrum. Cavitation is induced by a laser diode emitting at 810 nm wavelength with an output of 5 W (the pump laser), which is focused through a 25.4 mm focal length lens into the cuvette. Copper nitrate is highly absorptive of near-IR wavelengths, promoting thermocavitation, but is relatively transparent in the violet to yellow visible spectrum, where rhodamine B absorbs and fluoresces.

A 440 nm, 2 W diode (the exciter) is shaped into a sheet of approximately 1 cm width by a cylindrical plano-concave lens (f = -100 mm) in conjunction with an aspheric lens (f = 100 mm) and transmitted through the cuvette. The rhodamine B fluoresces within the exciter's light sheet, with fluorescence wavelengths typically in the range of 550-570 nm (green-yellow). A Miro m310 high speed video camera (Vision Research) records from perpendicular to the pump axis, through a longpass filter with cut-off wavelength of 550 nm, and a shortpass filter with a cut-off wavelength of 600 nm to block the pump. The camera uses several zoom lenses to enable a macro field of view of approximately 5 mm by 5 mm in the plane of fluorescence. Video is recorded at 1000 fps with 990 µs exposure time and 512 × 512 resolution.

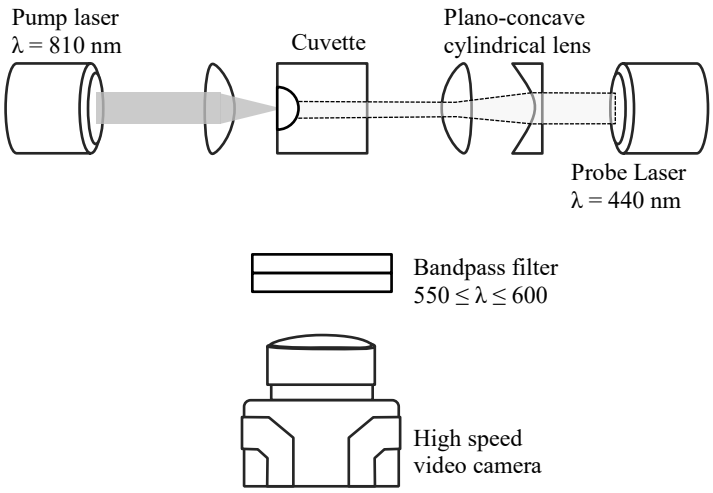

Figure 3 Experimental setup for laser-fluorescence temperature measurement.

The cavitation fluorescence solution consists of 4 mL of copper nitrate solution with rhodamine B dye added. The concentrations of copper nitrate and rhodamine B by weight used for temperature measurement are 0.48 g CN and 0.07 mg R-B to 1 g deionized water.

Raw images were digitally enhanced using ImageJ software. The images were cropped to remove the cuvette wall and areas outside of the excitation laser. The cropped image shows an area of approximately 3.5mm W × 6mm H centered on the irradiation axis. A sample frame is displayed in Figure 4.

To calibrate the fluorescence setup, the cuvette was filled with the rhodamine solution and heated to different temperatures on a hot plate. A thermocouple was used to verify the temperature of the liquid within the cuvette to ±1°C. 200 frames of video were recorded at each temperature. The video frames were divided into a 40 x 40 grid. The intensity of the fluorescence was measured within each cell of the grid and averaged for all 200 frames to establish a reference value for that temperature. A Python script was used for image analysis. Six temperatures were used to establish an intensity-temperature curve. Figure 5 shows the calibrated intensity curve for several grid squares, chosen at random.

Rhodamine B is reported in literature to vary approximately linearly with temperature. Sakakibara used a second-order least-squares fit and found near-linear temperature vs intensity [16]. Chen found good agreement with a linear fit as well [17].

The intensity curves for each grid square are closely approximated by a linear fit. The R^2 values remained consistently above 0.9 for all cells. The linear relationship agrees with findings in other applications of PLIF that used rhodamine B. The exact slope of the fit depends on the concentration of rhodamine, excitation power, and the optical setup. To prevent error due to slight variations in the optical setup between experiments, the calibration process was repeated after each experiment without touching the setup except to activate the hot plate.

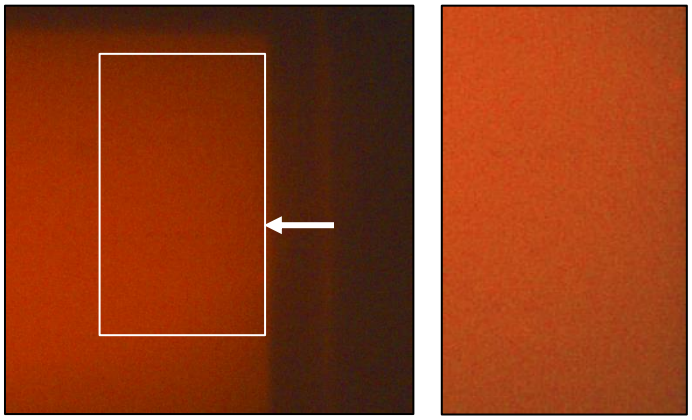

Figure 4 Raw experiment image (left) and processed image (right). The rectangular box indicates the cropped region. The white arrow indicates the pump laser axis.

The temperature was calculated using Equation 1.

$$T = m_{grid}\left(I - I_{ref,grid}\right) + T_{ref} \quad [1]$$

where T is the temperature, m_{grid} is the slope of the calibration line at that location within the grid, I is the R,G,B average value in that grid location and video frame, $I_{ref,grid}$ the R,G,B average for that grid location at the reference temperature, and T_{ref} the reference temperature.

It is worth noting that the concentration of rhodamine B in this study is far greater than typical PLIF applications use (typically on the order of 0.0001 mg rhodamine / g water). High video framerates necessitate short frame exposure times, minimizing the amount of light that can reach the camera sensor during each frame. Increased concentration of rhodamine B results in brighter fluorescence. However, there is

a red-shift in the fluorescence, as the rhodamine partially re-absorbs and re-emits its own light [18]. As such, the fluorescence is not at rhodamine B's nominal 550 nm emission peak, but rather between 560 and 600 nm. A bandpass filter of 550±10 nm blocked all excitation from the camera's view.

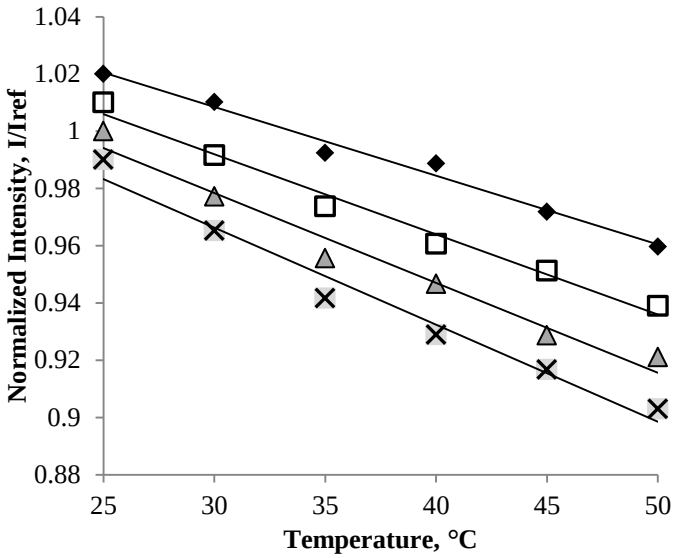

Figure 5 Fluorescent intensity versus temperature for typical grid cells in different locations within the image. The points indicate the normalized RGB value within that square. A linear fit is developed for each grid location. The squares are chosen at random.

One other consequence of the elevated rhodamine B concentration was the selection of excitation lasers. Rhodamine B has an absorption peak at approximately 540 nm; typically green-wavelength lasers are used to stimulate fluorescence. The increased concentration permitted a 520 nm beam to penetrate only approximately a millimeter into the liquid. The 440 nm probe laser was selected for its balance of transmission and absorption. It was able to pass through the entire cuvette exciting the rhodamine.

RESULTS

Shadowgraph Temperature Field

The results of the collapse of the bubble seen in Figure 1 can be observed, although not quantified, using a shadowgraph image where relative temperature differences can be seen as contours in the image. A series of still frames showing this process is depicted in Figure 7. After the bubble collapses, a stream of heated liquid is seen to migrate away from the boundary. Shadowgraphy does not quantify temperature but rather shows where temperature differences have altered the refractive index of the working fluid. As such, it is a useful tool for visualization but lacks the temperature quantification capability of PLIF.

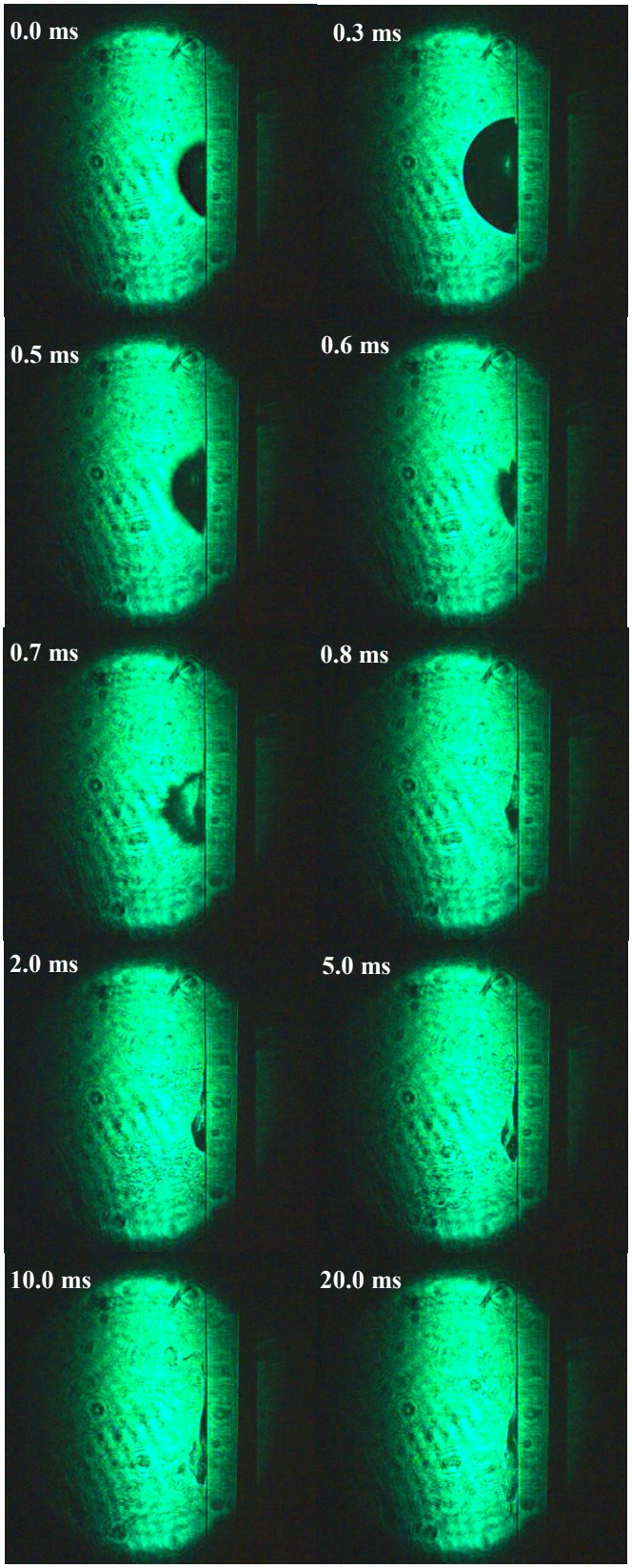

Figure 7 Shadowgraph images showing the ejection of hot liquid after cavitation bubble collapse. The labels indicate the length of time after the bubble nucleation.

Fluorescence Temperature Measurement

Temperature measurements were grouped chronologically into three phases: the heating phase, bubble phase, and mixing phase. The heating phase is defined as the time between the pump laser activation and bubble nucleation. The bubble phase lasts from the time the bubble appears until no bubble is visible for two consecutive video frames. In many cases, a cavitation bubble is observed to rebound from its initial collapse; for purposes of this study, the bubble phase is defined as including these subsequent bubble oscillation. The mixing phase starts after the bubble collapses until no motion is observed or a second bubble occurs.

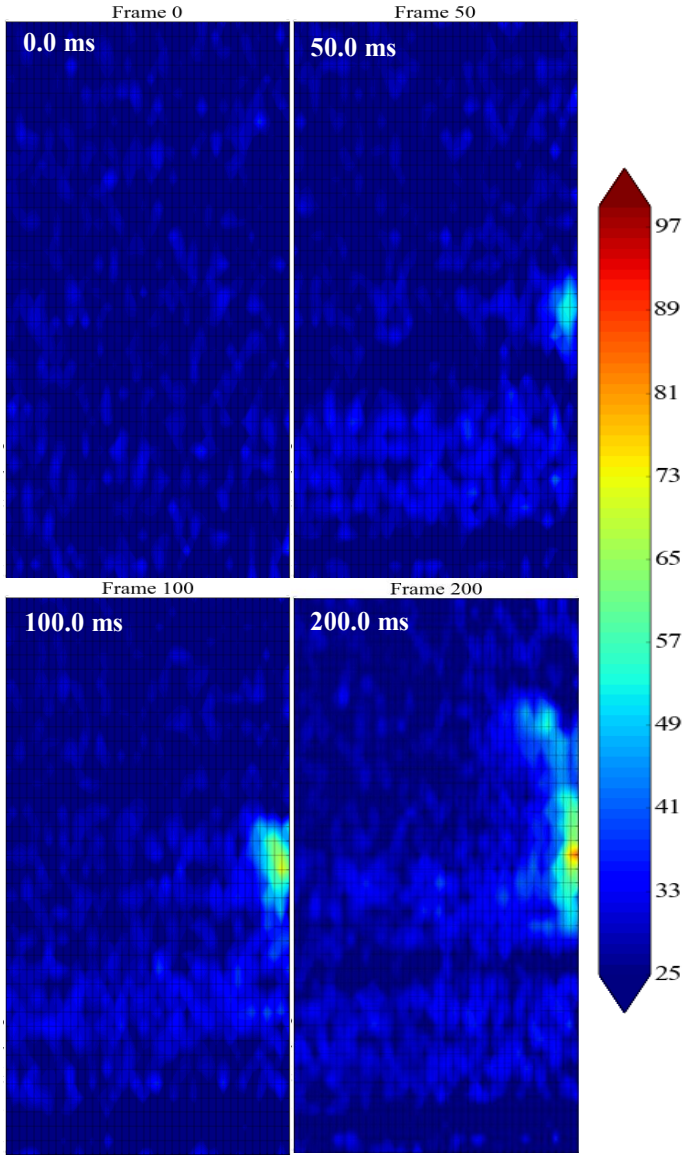

Figure 8 Temperature measurements during the heating phase, prior to bubble nucleation. The numbers represent the amount of time that has passed since the activation of the pump laser.

Heating

The heating phase for this study lasted approximately 262 ms, from the instant the laser was activated until the first bubble nucleated. Figure 8 shows selected frames from this period. During this time, the highest observed temperature was 105 °C. The thermal boundary layer is observed to start at the point of irradiation and spread vertically upwards, driven by natural convection. It gradually expands for approximately 260 ms after the laser is activated.

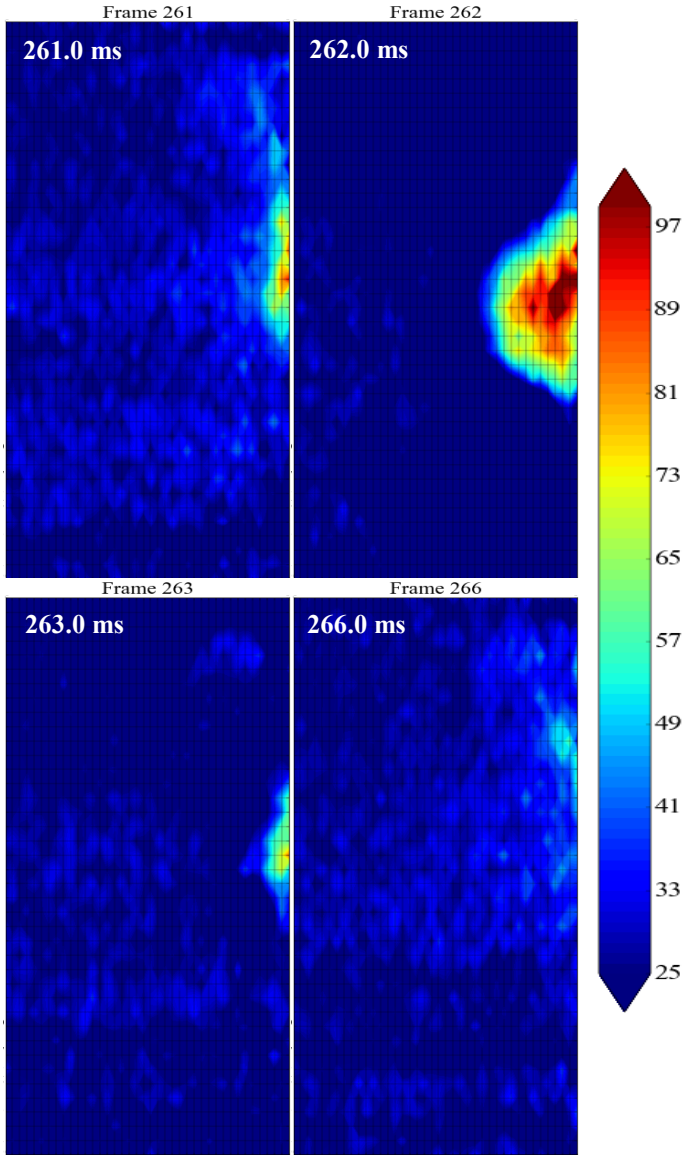

Figure 9 Temperature measurements during the bubble's growth, near its maximum diameter, and during its collapse.

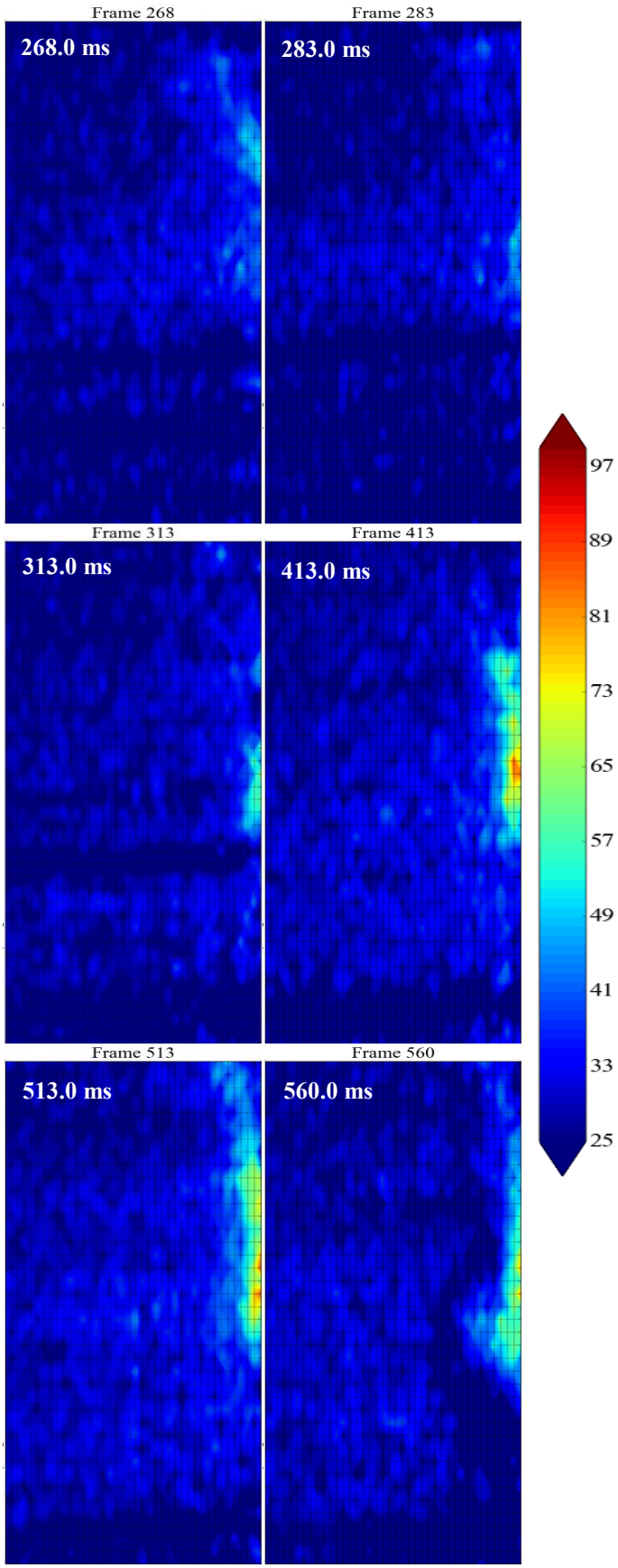

Figure 10 Temperature measurements during the mixing phase, after the collapse of the bubble.

Bubble

The heated liquid is driven outward by the growing bubble (Figure 9), reducing temperature at the heating point and dispersing the heated volume. The bubble itself appears as anomalous region – while it is undoubtedly quite hot, the temperature reported within the bubble is due to the absence of fluorescing substance, appearing very dark on video. Shortly after the bubble collapses, however, the thermal boundary layer appears nearly absent. A relatively small volume of hot liquid is seen ejected from the bubble site.

Mixing

The mixing phase extended from the collapse of the bubble for 292 ms, ending upon the formation of a new bubble. Thus, the mixing phase after one bubble is also the heating phase for the next. There is some difference in the length of heating phases between bubbles – this jitter is likely due to the relatively long focal length lens used in the experimental setup; Padilla-Martinez, et al, observed that increasing the energy density makes optical cavitation occur more consistently [5]. However, under continuous irradiation, the energy added to the liquid must be dispersed. The collapse of the cavitation bubble seems to account for this. Figure 10 depicts the mixing phase, showing the dispersion and regrowth of the thermal boundary layer and culminating in the second bubble.

CONCLUSION

The temperature field as it develops during optical thermocavitation has been studied. The thermal boundary layer arising from the laser-spot heating near the cuvette wall grows until a bubble nucleates. Because of the rapid heating and relatively small heated volume, the temperature is able to approach the spinodal temperature before explosive vaporization occurs. The growth and collapse of the bubble then disperses the heated liquid. Because most of the energy used to induce cavitation is converted from optical energy to sensible and latent heat and finally to mechanical and acoustic energy, the thermal boundary layer essentially disappears and regrows from ambient temperature.

This cooling effect facilitates cavitation as a targeted, non-intrusive, spot agitator to provide increased convective cooling to desired areas. Future work includes examining the dynamics of the thermal boundary layer in a liquid that is externally heated in addition to the laser's spot heating, and exploration of the growth of the thermal boundary layer over an extended period of time and through the occurrence of multiple sequential bubbles.

ACKNOWLEDGEMENTS

The authors would like to thank Vicente Robles, Ismael Martinez, and Ruddy Calderon for their laboratory assistance. This work is supported by NSF-CBET grant 1403508 and the UCMEXUS Dissertation Research Grant. Discussions with Dr. Santiago Camacho-Lopez, Dr. Juan-Pablo Padilla Martinez, Dr. Monica Martinez, Dr. Marko Princevac, and Dr. Lorenzo Mangolini have been invaluable in advancing this work.

REFERENCES

1. Lee, C.-Y., et al., *Microfluidic Mixing: A Review.* International Journal of Molecular Sciences, 2011. **12**: p. 3263-3287.
2. Liu, R.H., et al., *Bubble-induced acoustic micromixing.* Lab on a chip, 2002. **2**: p. 151-7.
3. Carome, E.F., N.A. Clark, and C.E. Moeller, *Generation of Acoustic Signals in Liquids by Ruby Laser-Induced Thermal Stress Transients.* Applied Physics Letters, 1964. **4**(6): p. 95-97.
4. Camacho-López, S., et al., *High Resolution Optical Experimental Technique for Computing Pulsed Laser Induced Cavitation Bubble Dynamics in a Single Shot.* Atomization and Sprays, 2013. **23**(6): p. 475-485.
5. Padilla-Martinez, J.P., et al., *Optic cavitation with CW lasers: A review.* Physics of Fluids, 2014. **26**(12): p. 1-12.
6. Prentice, P., et al., *Membrane disruption by optically controlled microbubble cavitation.* Nat Phys, 2005. **1**(2): p. 107-110.
7. Dijkink, R. and C.-D. Ohl, *Laser-induced cavitation based micropump.* Lab on a chip, 2008. **8**(10): p. 1676-1681.
8. Rastopov, S.F. and A.T. Sukhodolsky. *Sound generation by thermocavitation-induced cw laser in solutions*. in *Optical Radiation Interaction with Matter*. 1991. Leningrad, Russia: SPIE.
9. Huang, X., et al., *Controlled Manipulation and in Situ Mechanical Measurement of Single Co Nanowire with a Laser-Induced Cavitation Bubble.* Nano letters, 2010. **10**(10): p. 3846-51.
10. Fujimoto, J.G., et al., *Time-resolved studies of Nd:YAG laser-induced breakdown. Plasma formation, acoustic wave generation, and cavitation.* Investigative Ophthalmology & Visual Science, 1985. **26**(12): p. 1771-7.
11. Ramirez-San-Juan, J.C., et al., *Time-resolved analysis of cavitation induced by CW lasers in absorbing liquids.* Opt. Express, 2010. **18**(9): p. 8735-8742.
12. Rastopov, S.F. and A.T. Sukhodolsky, *Cluster nucleation in the process of CW laser induced thermocavitation.* Physics Letters A, 1990. **149**(4): p. 229-232.
13. Vogel, A. and W. Lauterborn, *Acoustic transient generation by laser-produced cavitation bubbles near solid boundaries*. Vol. 84. 1988: ASA. 719-731.
14. Padilla-Martinez, J.P., et al., *Breaking the Rayleigh-Plateau Limit Using Thermocavitation Within a Droplet.* Atomization and Sprays, 2013. **23**(6): p. 487-503.
15. Crimaldi, J.P., *Planar laser induced fluorescence in aqueous flows.* Experiments in Fluids, 2008. **44**(6): p. 851-863.
16. Sakakibara, J., K. Hishida, and M. Maeda, *Measurements of thermally stratified pipe flow using image-processing techniques.* Experiments in Fluids, 1993. **16**(2): p. 82-96.
17. Chen, Y.Y. and A.W. Wood, *Application of a temperature-dependent fluorescent dye (Rhodamine B) to the measurement of radiofrequency radiation-induced temperature changes in biological samples.* Bioelectromagnetics, 2009. **30**(7): p. 583-590.
18. Bindhu, C.V. and S.S. Harilal, *Effect of the Excitation Source on the Quantum Yield Measurements of Rhodamine B Laser Dye Studied Using Thermal-Lens Technique.* Analytical Sciences, 2001. **17**: p. 141-144.